

Polarization radiation of vortex electrons with large orbital angular momentum

Igor P. Ivanov^{1,2,*} and Dmitry V. Karlovets^{3,†}

¹*IFPA, Université de Liège, Allée du 6 Août 17, bâtiment B5a, 4000 Liège, Belgium*

²*Sobolev Institute of Mathematics, Koptyug avenue 4, 630090, Novosibirsk, Russia*

³*Tomsk Polytechnic University, Lenina 30, 634050 Tomsk, Russia*

(Dated: May 24, 2022)

Vortex electrons, i.e. freely propagating electrons whose wavefunction has helical wavefronts, could emerge as a novel tool for the physics of electromagnetic (EM) radiation. They carry non-zero intrinsic orbital angular momentum (OAM) ℓ and, for $\ell \gg 1$, a large OAM-induced magnetic moment, $\mu \approx \ell \mu_B$ (μ_B is the Bohr magneton), which affects the radiation of EM waves. Here, we consider in detail its influence on two forms of polarization radiation, namely on Cherenkov and transition radiation. Due to large ℓ , we can neglect quantum or spin-induced effects, which are of order $\hbar\omega/E_e \ll 1$, but retain the magnetic moment contribution $\ell\hbar\omega/E_e \lesssim 1$, which makes the quasiclassical approach to polarization radiation applicable. We discuss magnetic moment contribution to polarization radiation, which has never been experimentally observed, and study how its visibility depends on kinematical parameters and permittivity of the medium. In particular, it is shown that this contribution can, in principle, be detected in azimuthally non-symmetrical problems, for example when vortex electrons obliquely cross a metallic screen (transition radiation) or move nearby it (diffraction radiation). We predict left-right asymmetry of the transition radiation, which appears due to effective interference between the charge and the magnetic moment radiation fields. Numerical values of this asymmetry for vortex electrons with $E_e = 300$ keV and $\ell = \mathcal{O}(100 - 1000)$ are $\mathcal{O}(0.1 - 1\%)$, and we argue that this effect could be detected with today's technology. Finite conductivity of the target and a frequency dispersion play the crucial roles in these predictions.

PACS numbers: 41.60.Dk, 42.50.Tx

I. INTRODUCTION

Radiation of electromagnetic (EM) waves is an inherent property of charges. In electrodynamics, there exist two general classes of radiation: bremsstrahlung and polarization radiation (PR). Bremsstrahlung is produced by a charge accelerated in some external EM field and it comprises such processes as synchrotron radiation, undulator radiation, bremsstrahlung in a Coulomb field, etc. In contrast, various forms of polarization radiation such as Cherenkov radiation, transition radiation, diffraction radiation, Smith-Purcell radiation, parametric X-ray radiation, etc., can be emitted by a uniformly moving charge but only in the presence of a medium. In this case, at each point of a medium the time-dependent EM field of a moving particle induces time-dependent currents, which are sometimes called the polarization currents and may be considered as a source of radiation (see, e.g., [1–4]). In a microscopic treatment polarization radiation arises as a result of the so-called distant collisions of a particle with an atom or molecule. In this case, effective (mainly) dipole moments induced by a projectile's field inside a target emit only soft photons and the particle trajectory stays undisturbed, see e.g. [1–3].

It is clear that EM radiation can be produced not only by charges but also by neutral particles carrying higher multipoles: electric or magnetic dipoles, quadrupoles, etc. For example, there is a vast literature on the problem of the spin magnetic moment radiation in external fields and in matter (the so-called “spin light”) for electrons, neutrinos, etc. (see, e.g., [5–8] and references therein). Then, Cherenkov radiation by a neutron treated as a point-like particle with zero charge but with a magnetic dipole moment is a well-known problem (see e.g. [9, 10]). Transition radiation by magnetic moments as well as electric dipoles and quadrupoles also have been analyzed in detail in [10].

It is therefore remarkable that despite big theoretic interest, the experimental observations of influence of magnetic moment or any higher multipole on the EM radiation are very scarce. Putting aside various spin-dependent radiative processes in high-energy particle collisions, they are, in fact, limited to very few cases of bremsstrahlung of relatively energetic photons. For example, in [11], the intensity of the synchrotron radiation in the 100-400 keV range at the VEPP-4 storage ring for 5 GeV electrons was found to depend on the electron spin orientation. The magnitude of the effect was small, of order 10^{-4} – 10^{-3} , but due to photon high counting statistics it was well measurable. This effect

*E-mail: igor.ivanov@ulg.ac.be

†E-mail: d.karlovets@gmail.com

was even proposed as a tool to measure the beam transverse polarization at storage rings. Further development of this idea led to a proposal of a “spin-light polarimeter” for the future 12 GeV JLab storage ring [12]. Spin effects in bremsstrahlung were also observed at CERN by detecting GeV-range photons emitted by 35–243 GeV electrons passing through a tungsten single crystal (out of channeling regime) [13]. The effect was detectable due to the super-strong electromagnetic field in the crystal comparable with the Sauter-Schwinger limit in the electron rest frame.

In contrast with these results for bremsstrahlung, the magnetic moment (or any higher multipole) contribution to any form of *polarization radiation* has never been detected. There are several obstacles to this measurement. On the purely experimental side, a “no-win” situation: polarization radiation intensity is, roughly speaking, larger for soft photons, but the relative contribution of spin-induced magnetic moment is suppressed by $\hbar\omega/E_e$, where $\hbar\omega$ and E_e are the photon and electron energies. But even putting aside this experimental difficulty, there is a deeper problem of separating spin-induced magnetic moment contribution to polarization radiation from quantum recoil effects, which are of the same order. Indeed, in the macroscopic treatment of polarization radiation, one assumes that the particle’s trajectory is unperturbed by radiation. Thus, from the very beginning, one neglects the effects of order $\hbar\omega/E_e$, and the spin-induced magnetic moment contribution to polarization radiation lies beyond the standard quasiclassical calculation scheme. As for quantum theory of PR, the spin (or spin magnetic moment) contribution, again, has a natural competitor of the quantum recoil effects, which makes their experimental separation an almost hopeless task.

Theoretical prediction [14] and recent experimental demonstration of vortex electron beams [15–18] puts a dramatic twist on this problem. Vortex electrons carry intrinsic orbital angular momentum (OAM) ℓ with respect to their average propagation direction, and the values of ℓ can be rather large (up to 100 in [17] and up to 90 in [18]). The magnetic moment associated with OAM is correspondingly large, $\mu \approx \ell\mu_B$, where $\mu_B = e\hbar/2m_e c$ is the Bohr magneton [19]. It strongly enhances all the magnetic moment effects with respect to the usual spin contribution, $2\mu_B$. Using vortex electrons with $\ell \gg 1$, one can enter the regime in which magnetic-moment contribution is only moderately suppressed, $\propto \ell\hbar\omega/E_e \lesssim 1$, and remains much larger than quantum effects. This improves the visibility of the magnetic moment contribution to polarization radiation and, at the same time, makes its quasiclassical calculation a self-consistent problem. Observation of this contribution would be the first clear evidence of the PR by a multipole.

As a particular example, we considered in [20] transition radiation of vortex electrons with $\ell \gg 1$ obliquely incident on metallic foil and predicted that the OAM-induced magnetic moment contribution could manifest itself via left-right asymmetry of the emitted radiation. For electrons with $E_e = 300$ keV and $\ell \sim \mathcal{O}(1000)$ the asymmetry can be of order $\mathcal{O}(1\%)$, which must be well detectable. In this paper, we present a fuller discussion of this process, including dependence on the kinematical parameters and on the medium permittivity, as well as comparing it with Cherenkov radiation of vortex electrons.

The structure of the paper is the following. In Section II we remind the reader of the qualitative features of transition radiation from the charge and magnetic moment. We then pass to accurate description of the transition radiation from the system “charge + magnetic moment”, and present in Section III the formulas for two quasiclassical ways to model the magnetic moment. Numerical results are given in Section IV. In Section V we discuss the results and outline the requirements and strategy to detect the proposed effect in experiment.

II. TRANSITION RADIATION FROM “CHARGE + MAGNETIC DIPOLE”: QUALITATIVE FEATURES

A. General properties of PR

Polarization radiation (PR) occurs when a particle moves uniformly near or inside a medium with complex permittivity $\varepsilon(\omega) = \varepsilon' + i\varepsilon''$. As we are interested mostly in optical and UV spectral regions, one can set the magnetic permeability to one; this condition is justified for majority of real substances. Depending on the medium or target shape, one usually distinguishes different particular forms of PR: Cherenkov radiation (ChR), transition radiation (TR), diffraction radiation (DR), Smith-Purcell radiation (SPR), parametric X-ray radiation, etc (see, e.g., [2–4]). Along with the energy losses to excitation and ionization of atomic shells, which result in the discrete spectrum radiation of relatively *hard* photons (bremsstrahlung), there are also the so-called polarization losses related to the dipole moments induced inside the medium and leading to continuous spectrum radiation of relatively *soft* photons (see e.g. [3] and references therein). Although many *macroscopic* manifestations of PR were known since 1930-50’s (ChR, TR, DR, SPR), the *microscopic* quantum theory of PR explicitly demonstrating their common physical origin was developed only in the 1970-80’s by Amusia with co-workers (see e.g. [3, 21] and references therein; qualitative explanations of microscopic nature of, say, ChR were of course given before). The macroscopic approaches, in which such a unified nature of various radiation processes was explicitly demonstrated, have been developed only in recent years [2, 4, 22, 23].

As a matter of fact, radiation of soft photons (which is actually PR) represents somewhat complementary process

to the usual bremsstrahlung of an accelerated charge, since as we know only the *sum* of probabilities of these two processes is measured in experiment. One of the most remarkable differences between the ordinary bremsstrahlung and PR is that whereas intensity of the former is inversely proportional to the projectile (say, electron) mass squared, $dW \propto m_e^{-2}$, the intensity of the latter has no dependence on this mass at all. As a result, the PR can even dominate over the ordinary bremsstrahlung, especially in the ultrarelativistic case [2, 3].

Due to different kinematic conditions, various types of PR have different spectra but their shape, nevertheless, is mostly defined by the dispersion of permittivity. In particular, in ultrarelativistic case the spectrum (say, of TR [10]) can span up to the frequencies $\omega_c \sim \gamma\omega_p$ ($\gamma = E_e/m_e = 1/\sqrt{1-\beta^2}$ is the Lorentz factor) which, for very energetic electrons, can lie in X-ray region, since the plasma frequency ω_p is around 10 – 30 eV for many materials.

B. General properties of charge TR

One of the simplest and widely known types of PR is transition radiation, which occurs when a uniformly moving charge crosses a boundary separating two media with different permittivities. Put simply, although the motion of the charge is uniform, the accompanying electromagnetic field has to reorganize upon boundary crossing, and it is partly “shaken off” in the form of electromagnetic radiation. The simplest example of TR at normal incidence was considered in the seminal paper by Ginzburg and Frank [24]. In the following decades, a theory treating the physics of transition radiation in ever increasing details and in more general set-ups has gradually emerged, see e.g. [25] and also monograph [10], and even has become a standard textbook material [26]. There are several aspects which enrich the phenomenon of transition radiation and complicate its theoretical investigation: normal vs. oblique incidence, ideal conductor vs. a medium with arbitrary complex permittivity ε , one boundary vs. multiple boundaries (see e.g. [25]), etc.

One of the specific features of TR is radiation generation to both semispaces: the one the particle is coming from (backward TR) and the one the particle enters after crossing the boundary (forward TR), see Fig. 1, left. This can illustratively be explained as a radiation from two charges which annihilate at the interface (in order to comply with the boundary conditions) — from the original one (forward TR) and from its image (backward TR).

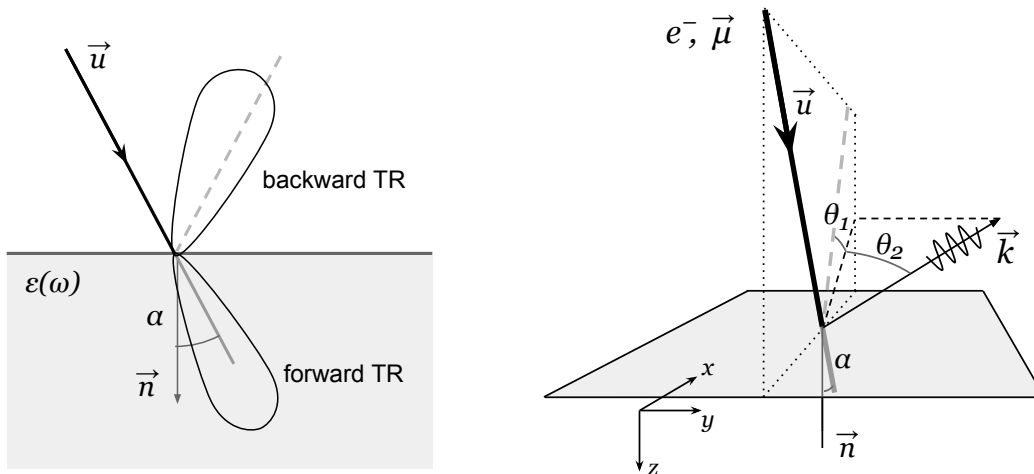


FIG. 1: (Left) Schematic view of the forward and backward TR lobes projected onto the incidence plane. (Right) Angle conventions for oblique incidence with the example of backward TR. The direction of specular reflection is shown by the gray dashed line.

In order to illustrate some of these features, let us consider a point-like charge (an electron) approaching from vacuum the flat boundary of a medium with a general ε , Fig. 1, right. We assume an oblique incidence with angle α between particle trajectory and the normal to the boundary. We then define the incidence plane and the direction of specular reflection. Any direction of the emitted photon can be characterized by two “flat” angles θ_1 and θ_2 describing out of plane deviation angle (θ_2) and the in-plane projection measured from the direction of specular reflection (θ_1).

The classical result of Ginzburg and Frank concerns the normal incidence, for which only one polar angle θ is needed. When solving TR problem for an oblique incidence, it is easier to work with the usual polar and azimuthal angles θ, ϕ , but the final result is more illustrative when expressed via the “flat” angles $\theta_{1,2}$. Below we shall use both

pairs of variables which are related as

$$\cos \theta = \cos \theta_2 \cos(\alpha + \theta_1), \quad \sin \phi = \frac{\sin \theta_2}{\sqrt{1 - \cos^2 \theta_2 \cos^2(\alpha + \theta_1)}}.$$

The general formula for the charge TR spectral-angular distribution of the emitted energy for oblique incidence on an ideally conducting ($\varepsilon'' \rightarrow \infty$) target is (this formula as well as others given below can be deduced from the expressions provided in Sec.III and they coincide with the familiar results of Refs. [10, 25])

$$\frac{d^2W}{d\omega d\Omega} = \frac{e^2}{\pi^2 c} \beta^2 \cos^2 \alpha \frac{(\sin \theta - \beta \sin \alpha \cos \phi)^2 + \beta^2 \sin^2 \alpha \cos^2 \theta \sin^2 \phi}{((1 - \beta \sin \alpha \sin \theta \cos \phi)^2 - \beta^2 \cos^2 \theta \cos^2 \alpha)^2}, \quad (1)$$

both for the forward and for the backward TR.

In the non-relativistic approximation and at normal incidence, it has a typical form for any dipole radiation:

$$\frac{d^2W}{d\omega d\Omega} \approx \frac{e^2}{\pi^2 c} \beta^2 \sin^2 \theta. \quad (2)$$

As the electron becomes relativistic, the angular dependence develops two prominent lobes near the forward and backward directions with the maxima at $\theta = \gamma^{-1} \ll 1$:

$$\frac{d^2W}{d\omega d\Omega} \approx \frac{e^2}{\pi^2 c} \frac{\theta^2}{(\gamma^{-2} + \theta^2)^2}. \quad (3)$$

At oblique incidence, the two lobes shift. The forward TR is located near the particle trajectory, while the backward lobe stays close to direction of specular reflection. In the relativistic case, $\theta_1, \theta_2, \gamma^{-1} \ll 1$, the angular distributions become slightly asymmetrical in the plane of incidence (direction quantified by θ_1), but stay symmetric (in the absence of magnetic moment) in the orthogonal plane:

$$\frac{d^2W}{d\omega d\Omega} \approx \frac{e^2}{\pi^2 c} \frac{\theta_1^2 + \theta_2^2}{(\gamma^{-2} + \theta_1^2 + \theta_2^2)^2} \frac{1}{(1 - \theta_1 \tan \alpha)^2}. \quad (4)$$

The typical width of the lobes in the wave zone is $\sim \gamma^{-1}$. Note that for moderately relativistic electrons, for example those produced in electron microscopes ($E_e = 300$ keV, $\beta \approx 0.8$), the lobes are rather wide and are sizably shifted with respect to the reference directions.

In a general case of a finite $\varepsilon(\omega)$, the radiation lobes in the backward/forward directions stay asymmetric in θ_1 but do not coincide. It happens, in particular, for almost transparent media due to possible contribution of the Cherenkov radiation in the forward direction. If the target is a good conductor, the energies emitted in the forward/backward directions coincide. However for a medium with weak absorption ($\varepsilon'' \ll \varepsilon'$), the reflectivity of the interface is small, so the forward TR dominates.

The spectrum of TR photons is mostly shaped by the dispersion of the medium, $\varepsilon(\omega)$. For forward TR (the energetic photons go in the forward direction only), below the critical frequency $\omega_c \sim \gamma \omega_p$ the spectrum stays roughly flat. Above the plasma frequency, $\omega \gg \omega_p$, the medium becomes increasingly transparent with a typical dependence $\varepsilon - 1 \propto 1/\omega^2$, which leads to a rather sharp cut-off in the spectrum when $\omega \gg \omega_c$. This implies that for moderately relativistic electrons TR detection beyond optical/UV spectral region is difficult.

C. TR from a magnetic moment

TR from a pointlike neutral particle carrying a non-zero magnetic moment was considered, for instance, in [10]. Theoretical description of this process invokes several delicate aspects. The first subtlety is that the magnetic moment can be modelled, classically, either as a close pair of magnetic monopoles or as a current loop of a small size. It is remarkable that in a generic situation (arbitrary orientation of the magnetic moment and arbitrary permeability of the medium) these two approaches lead to distinct results, both for TR energy and for polarization of the emitted radiation [10]. A similar ambiguity appears for Cherenkov radiation, see e.g. [9]. Therefore, it should be stressed that, in the absence of magnetic monopoles in Nature, we should always model magnetic moment by a current loop.

The second subtlety is that the electric and magnetic dipole moments are not invariant upon Lorentz boosts. In general, the electric and magnetic dipole moments transform as components of an antisymmetric tensor $M^{\mu\nu}$. If $\boldsymbol{\mu}$ is the magnetic moment in the particle rest frame, then upon a boost with velocity \mathbf{u} it generates an electric dipole moment $\mathbf{d} \parallel [\mathbf{u} \times \boldsymbol{\mu}]$. Fortunately, in the case of vortex electron beams the magnetic moment is parallel to the average

propagation direction, which eliminates the electric dipole moment contribution. The only effect then is a Lorentz contraction of the magnetic moment value from μ in the rest frame to μ/γ in the lab frame.

The main changes of the TR from a longitudinal pointlike magnetic dipole $\mu = \ell\mu_B$ with respect to the charge TR can be anticipated already from comparison between the respective currents: $\mathbf{j}_\mu = c \text{rot}[\boldsymbol{\mu}\delta(\mathbf{r} - \mathbf{u}t)]/\gamma$ vs. $\mathbf{j}_e = e \mathbf{u} \delta(\mathbf{r} - \mathbf{u}t)$. Rotor leads to an extra factor $i\omega/c$ in the Fourier components of the radiation field. As a result, the relative strength of the magnetic moment TR always bears the following small factor

$$x_\ell = \ell \frac{\hbar\omega}{E_e}. \quad (5)$$

The radiation energy contains this factor squared. For optical/UV photons and for typical electron energies achievable in an electron microscope, we get $x_\ell \sim 10^{-5}\ell$. Therefore, radiation of pure magnetic moments is suppressed by several orders of magnitude. Increasing ℓ partially compensates this suppression, but it still remains prohibitively difficult to detect.

As we shall demonstrate below, the general formula for the ‘‘pure’’ magnetic moment TR distribution for oblique incidence on an ideally conducting target (again identical for backward TR and forward TR) is

$$\left. \frac{d^2W}{d\omega d\Omega} \right|_\mu = \gamma^{-2} \frac{\mu^2}{\pi^2 c} \left(\frac{\omega}{c} \right)^2 \frac{\sin^2 \alpha \sin^2 \phi (1 - \beta \sin \alpha \sin \theta \cos \phi)^2 + \cos^2 \theta [\beta \sin \theta (1 - \sin^2 \alpha \sin^2 \phi) - \sin \alpha \cos \phi]^2}{[(1 - \beta \sin \alpha \sin \theta \cos \phi)^2 - \beta^2 \cos^2 \theta \cos^2 \alpha]^2}, \quad (6)$$

where $\gamma^{-1}\mu$ is the magnetic moment in the laboratory frame. Taken at face value, this expression does not vanish when $\beta \rightarrow 0$. However, as will become clear hereafter, it does for any finite $\varepsilon(\omega)$, which simply means that ideal conductor is a model. When $\mu \approx \ell\mu_B$, we have

$$\gamma^{-1} \frac{\mu\omega}{c} = \frac{1}{2} \varepsilon x_\ell$$

At normal incidence and in the ultrarelativistic case, we have the formula which is very similar to (3):

$$\left. \frac{d^2W}{d\omega d\Omega} \right|_\mu \approx \gamma^{-2} \frac{\mu^2}{\pi^2 c} \left(\frac{\omega}{c} \right)^2 \frac{\theta^2}{(\gamma^{-2} + \theta^2)^2}. \quad (7)$$

Finally, the relative intensity of the magnetic moment radiation, again at normal incidence, is

$$\left. \frac{d^2W}{d\omega d\Omega} \right|_\mu / \left. \frac{d^2W}{d\omega d\Omega} \right|_e = \left(\frac{\gamma^{-1}\mu\omega \cos \theta}{ec} \right)^2 \approx \frac{1}{4} x_\ell^2 \cos^2 \theta \ll 1 \quad (8)$$

For oblique incidence, angular distributions of magnetic moment TR are also asymmetric in the plane of incidence (with respect to θ_1), but stay symmetric in the perpendicular plane (in θ_2).

D. TR from charge + magnetic moment

Of course, in the case of electron, we deal with both charge and magnetic moment contributions to TR. Fields for both sources add up, and the radiated energy can contain three terms

$$dW = dW_e + dW_{e\mu} + dW_\mu, \quad (9)$$

describing the radiation energy of charge dW_e and of magnetic moment dW_μ as well as their interference $dW_{e\mu}$. The explicit equations for dW will be given in the next section.

If we want to detect TR from magnetic moment in a situation with extremely small dW_μ , we should focus on extracting the interference term $dW_{e\mu}$. This task turns out to be tricky due to a number of reasons. An analysis of situations when this interference is present was performed in [27].

First, the emitted energy is a 3-scalar while μ is a pseudovector. Therefore, the interference term must contain a triple product $\mathbf{e}_k \cdot [\boldsymbol{\mu} \mathbf{n}]$, where \mathbf{e}_k is the direction of the emitted photon and \mathbf{n} is the boundary normal. This triple product vanishes for normal incidence, while for oblique incidence it changes sign upon $\theta_2 \rightarrow -\theta_2$ (i. e. by flipping the sign of the out-of-plane component of \mathbf{e}_k). Therefore, the interference can be observed only at oblique incidence and only in differential distribution, not in total energy.

Since the interference term is small compared with the pure charge radiation, the angular distribution will also contain two lobes in the forward/backward direction, but they will be slightly non-symmetric under $\theta_2 \rightarrow -\theta_2$. A convenient way to quantify this distortion is to calculate the asymmetry

$$A(\alpha, \omega, \ell) = \frac{\int d\Omega f(\theta_2) \frac{d^2W}{d\omega d\Omega}}{\int d\Omega |f(\theta_2)| \frac{d^2W}{d\omega d\Omega}}. \quad (10)$$

where $f(\theta_2)$ is some function, odd in $\theta_2 \rightarrow -\theta_2$. The simplest choice, $f(\theta_2) = \text{sgn}(\theta_2)$, yields the widely used expression

$$A = \frac{\int d\Omega_L \frac{d^2W}{d\omega d\Omega} - \int d\Omega_R \frac{d^2W}{d\omega d\Omega}}{\int d\Omega_L \frac{d^2W}{d\omega d\Omega} + \int d\Omega_R \frac{d^2W}{d\omega d\Omega}}. \quad (11)$$

Here, $d\Omega_L$ and $d\Omega_R$ indicate two hemispheres lying to the left and to the right from the incidence plane. In fact, these integration domains do not have to cover the entire hemispheres, but in any case they must be symmetric under $\theta_2 \rightarrow -\theta_2$. Alternative definitions of asymmetry, in which one weights the angular distribution, say, with a function $f(\theta_2) = \sin \theta_2$, can also be employed. Below we shall use the definition (11) unless explicitly mentioned otherwise.

There is yet another factor that can suppress interference. Note that the rotor present in the definition of \mathbf{j}_μ produces an extra i factor in the Fourier-components. As a result, the radiation field will contain the magnetic moment contribution with a relative phase:

$$\mathbf{H}^R = \mathbf{H}_e^R + \mathbf{H}_\mu^R = a + ix_\ell b, \quad (12)$$

with some quantities a and b . These two quantities are, generally speaking, complex due to complex ε (or, to be more accurate, due to complex $\sqrt{\varepsilon}$). However if they have equal phases, the interference term $dW_{e\mu}$ vanishes. This happens, in particular, in two limiting cases: $\text{Im} \varepsilon = 0$ (transparent medium) and $\text{Im} \varepsilon = \infty$ (an ideal conductor). Therefore, in order to get a non-zero asymmetry, we must consider a real medium with a sizable (but not asymptotically large) $\text{Im} \varepsilon$.

If all these conditions are satisfied, we can expect, very roughly, the asymmetry (11) of the order of $A \sim x_\ell$. For the typical experiments with vortex electrons in microscopes, this amounts to $A \sim \mathcal{O}(1\%)$ for optical/UV TR from electrons with $\ell \sim \mathcal{O}(1000)$, and proportionally weaker asymmetries for smaller ℓ .

This makes detection of the asymmetry a rather delicate experimental undertaking. It necessitates a careful numerical analysis of the effect, which we perform below. It will allow us to obtain a reliable numerical results for realistic set-ups and to check how this asymmetry can be enhanced.

We end this section by mentioning that there exists alternative suggestion to detect the effect of large OAM in transition radiation, [28], which relies on recent calculations [27]. In this method, the quantity of interest is not the angular distribution of emitted photons but their polarization. Without magnetic moment contribution, the emitted photons are linearly polarized. Presence of magnetic moment leads to a slightly elliptic polarization for the off-plane photons. If one manages to measure the polarization of the photons very close to the direction of minimum intensity, the degree of circular polarization can be sizable, of the level of few percent or higher for $\ell = 100$. Whether such an accurate angular selection is feasible in realistic devices, remains to be studied.

III. TR FROM VORTEX ELECTRONS: QUANTITATIVE DESCRIPTION

A. Vortex electrons

Vortex electron state is a freely propagating electron whose wave function contains phase singularities with non-zero winding number ℓ . Such electron state is characterized, simultaneously, by an average propagation direction and an intrinsic orbital angular momentum (OAM) with projection $L = \hbar\ell$ on this direction. Following suggestion [14], vortex electrons were recently created in experiments by several groups, [15–18]. They are produced in electron microscopes with typical energy of $E_e = 200 - 300$ keV with the aid of computer generated diffraction gratings, which induce ℓ as large as 25 in the first diffraction peak and proportionally larger ℓ in faint higher diffraction peaks. These vortex electrons can be accurately manipulated and in particular can be focused to a spot of angstrom size [29].

The simplest example of a vortex state for a spinless particle is given by the Bessel beam state [30, 31] whose coordinate wave function is

$$\psi(r_{\perp}, \phi_r, z) \propto e^{ik_z z} e^{i\ell\phi_r} J_{\ell}(k_{\perp} r_{\perp}). \quad (13)$$

At large ℓ , the properties of Bessel functions lead to a narrow radial distribution located around $r_{\perp} \approx \ell/k_{\perp}$, in a good correspondence with quasiclassical picture of such an electron as a rotating ring of electronic density.

The spin degree of freedom for a vortex electron can also be included [19, 31]. Spin and OAM degrees of freedom interact [19], and both of them induce magnetic moment of the vortex electron (in the lab frame)

$$\frac{\mu}{\gamma} = (\ell + 2s - \Delta s) \frac{\mu_B}{\gamma} \approx \ell \frac{\mu_B}{\gamma}, \quad (14)$$

which was confirmed by observation of the OAM-dependent Larmor precession in the longitudinal magnetic field, [32]. Here Δs is an effective shift in magnetic moment due to spin-orbital interaction in vortex electron. In the case of large ℓ , which concerns us in this paper, we can neglect the spin contribution, which is indicated in the last expression in (14). The OAM-induced magnetic moment in this approximation is aligned with the average propagation direction of the vortex electron regardless of the spin state.

B. Modelling large OAM-induced magnetic moment

An electron vortex state is characterized by a non-trivial spatial structure of the wave function. In this sense, it is an inherently quantum state. However, as we explained in the introduction, the large value of ℓ allows one to treat polarization radiation from the OAM-induced magnetic moment quasiclassically neglecting the quantum effects during radiation, because the former is governed by the ratio $\ell\hbar\omega/E_e$ while the latter is of order $\hbar\omega/E_e$.

Not only does the magnetic moment (14) describe how vortex electrons couple to an external longitudinal magnetic field, but it is also a source of its own electromagnetic field. Therefore, if the vortex electron wavepacket is sufficiently compact, it can be modelled as a classical *point-like* source with charge e and an *intrinsic* magnetic moment μ given by (14), Fig. 1. This picture is behind our first method to calculate TR from vortex electrons passing from one medium into another. In this purely phenomenological model, we do not discern the internal microscopic structure of the vortex electron nor do we specify the origin of the large magnetic moment. The only assumption we make is that, in the absence of magnetic monopoles, the magnetic moment arises only from closed charge current loops.

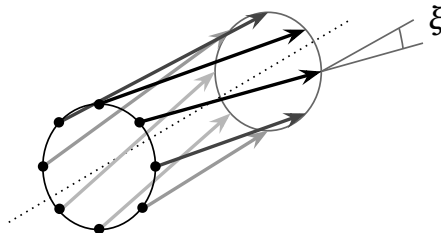


FIG. 2: Modelling magnetic moment of a vortex electron via a flat rotating annular bunch of point charges.

To control the validity of this approach, we devised our second model, which also treats the vortex electron quasiclassically but in which the OAM-induced magnetic moment becomes an *emergent* quantity.

In this model, we calculate *coherent* transition radiation from a very short (“flat”) bunch of a large number of electrons, $N \gg 1$, which carry no intrinsic magnetic moment and whose trajectories are straight rays passing at fixed skew angles through a ring of a microscopic size $R \ll \lambda$, Fig. 2. Individual charges move at constant and equal longitudinal velocities and have equal z coordinates, so that at any given time they form an infinitely thin annular slab in the transverse plane. It then becomes the standard calculation of a coherent TR from a compact bunch with the only exception that the total charge in the bunch is just e (in other words, we calculate the coherent radiation energy of a bunch and divide the energy by N^2). Note that this thin ring model is qualitatively similar to the true transverse wave function profile of a large- ℓ vortex electron mentioned above.

In order to compare the two models, we need to determine the effective ℓ within the second approach. This can be done quasiclassically as

$$\ell_{\text{eff}} = \frac{Rp \sin \xi}{\hbar}, \quad (15)$$

where p is the electron momentum and ξ is the skew angle, so that $p \sin \xi$ is the absolute value of the transverse momentum of each electron in the bunch. The same expression can be also obtained from the definition of the magnetic moment of a current loop with an area S and a current I

$$\ell_{\text{eff}} = \frac{\mu}{\mu_B} = \frac{2m_e c}{e\hbar} \gamma \pi R^2 \frac{ev \sin \xi}{2\pi R c} = \frac{Rp \sin \xi}{\hbar}. \quad (16)$$

As usual, μ refers to the magnetic moment in the rest frame, while the expression SI/c gives the magnetic moment in the lab frame.

These models can be applicable to a realistic experimental set-up with vortex electrons, if certain coherence conditions are satisfied. First, the quasiclassical treatment of the electrons as point-like particles in the transverse space is valid only if the vortex electrons are focused in a spot with a size much smaller than the emitted light wavelength λ . Within the second model, we also assume that the size of the ring is smaller than λ in order to improve coherence of the emitted light.

The same applicability condition requires also that the longitudinal extent of the individual electron wave function is much shorter than λ . This extent can be quantified by the longitudinal coherence length of the electron beam, that is, self-correlation length of the electron beam. This length is related to the monochromaticity of the electron beam and it can be found experimentally by counting the number of fringes in an electron diffraction experiment. The longitudinal compactness condition implies that the monochromaticity should not be too good.

Finally, the calculations of TR below are performed for individual electrons, not electron bunches because we assume that successive electrons pass through the foil one at a time. This implies that they must be separated by distances much larger than λ , which in turn restricts the current to values below $\sim 10 \mu\text{A}$. This is satisfied by a large margin in experiments with vortex beams realized so far.

If the above coherence requirements are all fulfilled, the two models are expected to yield qualitatively similar and numerically close results, because the second model proposes a microscopic origin of the large magnetic moment introduced “by hand” in the first model. We note that for the simple case of normal incidence and pure magnetic moment (no charge) a similar expectation was explicitly mentioned and verified in chapter 3.7 of [10].

C. Methodical example: Cherenkov radiation from charge + intrinsic magnetic moment

We start with the simpler case of Cherenkov radiation of vortex electrons with large OAM-induced magnetic moments, which is calculated according to the first model.

We consider a point-like particle with a charge e and an intrinsic magnetic moment, which in the particle rest frame is equal to $\boldsymbol{\mu}$ and directed along the velocity. The charge and current densities in the rest frame in vacuum are

$$\rho_e = e\delta(\mathbf{r}), \quad \mathbf{j}_\mu = c \text{rot}[\boldsymbol{\mu}\delta(\mathbf{r})]. \quad (17)$$

Note that this expression is valid for the case when the magnetic moment originates from current loops.

In the lab frame, the currents are

$$\mathbf{j}_e = e\mathbf{u}\delta(\mathbf{r} - \mathbf{u}t), \quad \mathbf{j}_\mu = \frac{c\boldsymbol{\mu}}{\gamma} \begin{pmatrix} \partial_y \\ -\partial_x \\ 0 \end{pmatrix} \delta(\mathbf{r} - \mathbf{u}t). \quad (18)$$

Note that the Lorentz transformation induced decrease of the magnetic moment in the lab frame. Their Fourier-transforms[38] are

$$\mathbf{j}_e(\mathbf{q}, \omega) = \frac{e}{(2\pi)^3} \mathbf{u} \delta(\omega - \mathbf{q} \cdot \mathbf{u}), \quad \mathbf{j}_\mu(\mathbf{q}, \omega) = \frac{ic}{(2\pi)^3} \mathbf{e}_\mu \delta(\omega - \mathbf{q} \cdot \mathbf{u}), \quad (19)$$

where

$$\mathbf{e}_\mu = \frac{\boldsymbol{\mu}}{\gamma} \begin{pmatrix} q_y \\ -q_x \\ 0 \end{pmatrix}. \quad (20)$$

Note the all-important i factor in the magnetic moment contribution.

These currents generate electric fields which determined by the Maxwell equations. Generically, their Fourier components are

$$\mathbf{E}(\mathbf{q}, \omega) = \frac{4\pi i}{\omega} \frac{1}{\mathbf{q}^2 - \omega^2/c^2} \left[\left(\frac{\omega}{c}\right)^2 \mathbf{j}(\mathbf{q}, \omega) - \mathbf{q} (\mathbf{q} \cdot \mathbf{j}(\mathbf{q}, \omega)) \right]. \quad (21)$$

According to the polarization currents approach developed in [4], the radiation field in the wave zone is found as

$$\mathbf{H}^R(\mathbf{r}, \omega) = (2\pi)^3 \left(\frac{\omega}{c}\right)^2 \frac{\varepsilon - 1}{4\pi} \frac{e^{i\sqrt{\varepsilon}r\omega/c}}{r} \mathbf{e}_k \times (\mathbf{E}_e(\mathbf{k}, \omega) + \mathbf{E}_\mu(\mathbf{k}, \omega)) = \quad (22)$$

$$= i \frac{\omega^2}{c^3} (\varepsilon - 1) \frac{e^{i\sqrt{\varepsilon}r\omega/c}}{r} \frac{\delta(\omega - \mathbf{k} \cdot \mathbf{u})}{\mathbf{k}^2 - \omega^2/c^2} \mathbf{e}_k \times \left[e\mathbf{u} + ic \frac{\mu}{\gamma} \mathbf{k} \times e_u \right], \quad (23)$$

and the argument of the delta-function turns into zero under the Cherenkov condition, $1 = \beta\sqrt{\varepsilon} \cos \theta_m$. Here, $\mathbf{e}_u = \mathbf{u}/u = (0, 0, 1)$ and $\mathbf{k} = \omega \mathbf{e}_k/c = \omega\sqrt{\varepsilon}(\sin \theta_m \cos \phi, \sin \theta_m \sin \phi, \cos \theta_m)/c$ is the wave vector. Calculating the radiated energy as

$$\frac{d^2W}{d\omega d\Omega} = \frac{cr^2}{\sqrt{\varepsilon}} |\mathbf{H}^R|^2, \quad (24)$$

we evaluate the squared delta-function in the usual way,

$$\delta^2(\omega - \mathbf{k} \cdot \mathbf{u}) \rightarrow \delta(\omega - \mathbf{k} \cdot \mathbf{u})\delta(0) \rightarrow \frac{T}{2\pi} \delta(\omega - \mathbf{k} \cdot \mathbf{u}),$$

where T is a large ($T \gg \omega^{-1}$) period of time. Integrating the resultant expression over angles we note that the delta-function zero lies on the integration path only if the permittivity ε is real ($\varepsilon'' = 0$). In that case we come finally to:

$$\frac{1}{uT} \frac{dW}{d\omega} = \frac{e^2}{c^2} \omega \left(1 - \frac{1}{\beta^2 \varepsilon}\right) \left[1 + \left(\frac{\mu\omega\sqrt{\varepsilon}}{eu\gamma}\right)^2\right]. \quad (25)$$

This is the Tamm-Frank formula for Cherenkov radiation with contribution of a magnetic moment. As predicted, there is no interference term, $dW_{e\mu}$, due to transparency of the medium being considered.

It should be noted however that this term is absent even in absorbing medium. Indeed, for a medium with weak absorption (otherwise, the Cherenkov radiation problem itself has no sense whatsoever), the radiation field squared is proportional to (here $\kappa \equiv \text{Im}\sqrt{\varepsilon}$)

$$\left| \mathbf{e}_k \times [e\mathbf{u} + ic\gamma^{-1}\mu \mathbf{k} \times e_u] \right|^2 \propto (eu \sin \phi - \kappa\gamma^{-1}\mu\omega \cos \theta \cos \phi)^2 + (eu \cos \phi + \kappa\gamma^{-1}\mu\omega \cos \theta \sin \phi)^2 \quad (26)$$

and the terms linear in μ cancel each other. This remarkable feature obviously is due to azimuthal symmetry of the problem. This is not the case for transition radiation in the oblique incidence geometry, which we are now going to demonstrate.

D. Radiation field for TR from charge + intrinsic magnetic moment

Now we consider TR generated by oblique passage of a particle with a charge and magnetic moment through a flat boundary between the vacuum and a non-magnetic medium with (complex) permittivity $\varepsilon(\omega)$. Axis z is chosen as a normal to the boundary, and axis x defines the particle incidence plane. The particle approaches the boundary in the (x, z) plane at the angle α to the normal, and its velocity is $\mathbf{u} = u(\sin \alpha, 0, \cos \alpha)$.

In the lab frame, the currents are

$$\mathbf{j}_e = e\mathbf{u} \delta(\mathbf{r} - \mathbf{u}t), \quad \mathbf{j}_\mu = \frac{c\mu}{\gamma} \begin{pmatrix} \cos \alpha \partial_y \\ \sin \alpha \partial_z - \cos \alpha \partial_x \\ -\sin \alpha \partial_y \end{pmatrix} \delta(\mathbf{r} - \mathbf{u}t). \quad (27)$$

Their Fourier-transforms stay the same, (19), with

$$\mathbf{e}_\mu = \frac{\mu}{\gamma} \begin{pmatrix} \cos \alpha q_y \\ \sin \alpha q_z - \cos \alpha q_x \\ -\sin \alpha q_y \end{pmatrix}. \quad (28)$$

In the problem of calculating TR, we deal with a situation which is homogeneous along coordinates x and y , but not z due to the presence of a boundary. Therefore, it is convenient to work with partial Fourier transforms $\mathbf{E}(\mathbf{q}_\perp, z, \omega)$,

with $\mathbf{q}_\perp = (q_x, q_y, 0)$ in which the dependence on z is kept. Due to linearity, the electric field (21) is a sum of contributions from both currents (19), which can be written as

$$\mathbf{E}_e(\mathbf{q}_\perp, z, \omega) = i \frac{2e}{(2\pi)^2 \omega u_z} \frac{e^{iz(\omega - \mathbf{q}_\perp \cdot \mathbf{u})/u_z}}{\mathbf{q}_\perp^2 + (\omega - \mathbf{q}_\perp \cdot \mathbf{u})^2/u_z^2 - \omega^2/c^2} \left[\left(\frac{\omega}{c}\right)^2 \mathbf{u} - \omega \left(\mathbf{q}_\perp + \mathbf{n}_z \frac{\omega - \mathbf{q}_\perp \cdot \mathbf{u}}{u_z} \right) \right], \quad (29)$$

$$\begin{aligned} \mathbf{E}_\mu(\mathbf{q}_\perp, z, \omega) = & - \frac{2e}{(2\pi)^2 \omega u_z} \frac{e^{iz(\omega - \mathbf{q}_\perp \cdot \mathbf{u})/u_z}}{\mathbf{q}_\perp^2 + (\omega - \mathbf{q}_\perp \cdot \mathbf{u})^2/u_z^2 - \omega^2/c^2} \times \\ & \times \left[\left(\frac{\omega}{c}\right)^2 \mathbf{e}_\mu - \left(\mathbf{q}_\perp + \mathbf{n}_z \frac{\omega - \mathbf{q}_\perp \cdot \mathbf{u}}{u_z} \right) \left(\mathbf{q}_\perp \cdot \mathbf{e}_\mu + \frac{\omega - \mathbf{q}_\perp \cdot \mathbf{u}}{u_z} e_{\mu,z} \right) \right], \end{aligned} \quad (30)$$

where $\mathbf{n}_z = (0, 0, 1)$ and \mathbf{e}_μ is given by (28).

In order to calculate the field of TR in the wave zone, we use the same polarization current technique. The radiation field can be written as

$$\mathbf{H}^R(\mathbf{r}, \omega) = \left(\frac{2\pi\omega}{c}\right)^2 \frac{\varepsilon - 1}{4\pi} \frac{e^{i\sqrt{\varepsilon}r\omega/c}}{r} [\mathbf{e}_k \times \mathcal{J}], \quad (31)$$

where

$$\mathcal{J} = \int dz' e^{-iz'k_z} [\mathbf{E}_e(\mathbf{k}_\perp, z', \omega) + \mathbf{E}_\mu(\mathbf{k}_\perp, z', \omega)], \quad (32)$$

is a quantity proportional to the polarization current [4]. We introduced here the ‘‘on-shell’’ wave vector in medium $\mathbf{k} = \mathbf{e}_k \omega/c$, where

$$\mathbf{e}_k = \sqrt{\varepsilon} \begin{pmatrix} \sin \theta_m \cos \phi \\ \sin \theta_m \sin \phi \\ \cos \theta_m \end{pmatrix} = \begin{pmatrix} \sin \theta \cos \phi \\ \sin \theta \sin \phi \\ \pm \sqrt{\varepsilon - \sin^2 \theta} \end{pmatrix}. \quad (33)$$

The two expressions in (33) relate the emission angle in medium θ_m with the emission angle θ in vacuum. Integration in (32) is carried out from 0 to ∞ for backward TR (in this case $e_{k,z} < 0$) and from $-\infty$ to 0 for forward TR ($e_{k,z} > 0$).

The radiation field can be conveniently written in the coordinates related not with the electron incidence plane, but with photon production plane (\mathbf{e}_k, z) . The radiation field (31) is orthogonal to \mathbf{e}_k and therefore has two components which lie in the production plane, H_{in}^R , and out of that plane, H_{out}^R . In the vacuum variables, they are expressed as

$$H_{out}^R = H_y^R \cos \phi - H_x^R \sin \phi, \quad H_{in}^R = \frac{1}{\sqrt{\varepsilon}} [-H_z^R \sin \theta \pm (H_x^R \cos \phi + H_y^R \sin \phi) \sqrt{\varepsilon\theta}]. \quad (34)$$

where we introduced short notation

$$\sqrt{\varepsilon\theta} \equiv \sqrt{\varepsilon - \sin^2 \theta}$$

The final expressions for these two components are

$$\begin{aligned} H_{out}^R = & \mathcal{N} \left[\sin \theta (1 - \beta^2 \cos^2 \alpha - \beta \cdot \mathbf{e}_k) \pm \beta^2 \sin \alpha \cos \alpha \cos \phi \sqrt{\varepsilon\theta} \right. \\ & \left. + i\mu \frac{\omega}{e\gamma c} \sin \alpha \sin \phi \left(\beta \cos \alpha \sin^2 \theta \mp \beta \sin \alpha \sin \theta \cos \phi \sqrt{\varepsilon\theta} \pm \sqrt{\varepsilon\theta} \right) \right], \end{aligned} \quad (35)$$

$$H_{in}^R = \mathcal{N} \sqrt{\varepsilon} \left[\beta^2 \sin \alpha \cos \alpha \sin \phi + i\mu \frac{\omega}{e\gamma c} [\beta \sin \theta (1 - \sin^2 \alpha \sin^2 \phi) - \sin \alpha \cos \phi] \right], \quad (36)$$

where the overall factor in front of the brackets is

$$\begin{aligned} \mathcal{N} = & \pm \frac{e}{2\pi c} (\varepsilon - 1) \beta \cos \alpha \frac{e^{i\sqrt{\varepsilon}r\omega/c}}{r} \times \\ & \times \left[(1 - \beta \sin \alpha \sin \theta \cos \phi)^2 - (\beta \cos \alpha \cos \theta)^2 \right]^{-1} \left[1 - \beta \sin \alpha \sin \theta \cos \phi \mp \beta \cos \alpha \sqrt{\varepsilon\theta} \right]^{-1}. \end{aligned} \quad (37)$$

As before, the upper and lower signs in these expressions correspond to the forward and backward radiation, respectively.

The spectral-angular distributions of the radiated energy can be found from the reciprocity theorem as follows [4]:

$$\frac{d^2W}{d\omega d\Omega} = 4cr^2 \cos^2 \theta \left(\left| \frac{1}{\varepsilon \cos \theta + \sqrt{\varepsilon\theta}} \right|^2 |H_{out}^R|^2 + \left| \frac{1}{\sqrt{\varepsilon}(\cos \theta + \sqrt{\varepsilon\theta})} \right|^2 |H_{in}^R|^2 \right). \quad (38)$$

Substituting here the explicit expressions for the radiation field and sorting out the charge and magnetic moment contributions, one can break the energy into the pure charge dW_e and pure magnetic moment dW_μ contributions as well as the interference term $dW_{e\mu}$, (9).

It can be easily checked that for a neutral particle with magnetic moment only and for ideally conducting surface the resultant formula coincides with Eq.(6).

We are interested in detecting the small contribution of the magnetic moment to radiation energy. There is a number of features which are visible directly in the above equations. Firstly, with the value of the intrinsic magnetic moment (14) and neglecting the spin contribution, one sees that the interference term is indeed suppressed by the factor $x_\ell \ll 1$, while the pure magnetic moment contribution is $\propto x_\ell^2$. For optical/UV photons and for typical electron energies achievable in an electron microscope, we get $x_\ell \sim 10^{-5}\ell$. This estimate makes it clear that one can only hope to detect the interference term $dW_{e\mu}$. Secondly, it is seen this interference term can originate only from $|H_{out}^R|^2$ and only with non-trivially complex ε . In particular, this interference term is absent for transparent medium, $\text{Im } \varepsilon = 0$, (similarly to the Cherenkov radiation case) and for the ideal conductor, $\text{Im } \varepsilon = \infty$. Finally, this term also vanishes for normal incidence ($\alpha = 0$) at any emission angles as well as at oblique incidence for emission in the incidence plane, $\phi = 0$.

We would like to emphasize that when applying the polarization current approach to TR problem, the current itself is taken as if the medium were boundaryless, $\mathbf{j} = \sigma(\mathbf{E}_e + \mathbf{E}_\mu)$, with σ being complex conductivity. Besides, the Green's function pole is shifted, $\omega/c \rightarrow \sqrt{\varepsilon}\omega/c$, because of effective "dressing" of the particle's field in the medium (see, e.g., [33]). The effects of boundary (or boundaries) are taken into account when we find how this (bare) current's field, which is calculated by integrating the current over the target's volume, changes due to reflections and refractions at them. By applying the reciprocity theorem, we reduce the initial (rather complicated) problem to the *complementary* problem of refraction, which is much easier to solve by using the usual Fresnel laws and summing up all the secondary re-reflected fields inside the target. The necessity of using the reciprocity theorem may be argued, in fact, by the causality considerations, which require permittivity $\varepsilon(\omega)$ to be always complex quantity, at least $\varepsilon = \varepsilon' + i0$; see also [34].

It should be noted that when considering TR at grazing incidence of not very energetic electrons, the applicability conditions of macroscopic electrodynamics may be violated [35]. So, the region where the models being used work well is determined by the following inequality

$$\frac{u_z}{\omega - (\mathbf{k}_\perp \mathbf{u})} = \frac{\lambda}{2\pi} \frac{\beta \cos \alpha}{1 - \beta \sin \alpha \cos \theta_2 \sin(\alpha + \theta_1)} \gg b$$

where b is the interatomic distance ($\sim 1 \text{ \AA}$). For the optical/near-UV region and parameters considered below, the left-hand side of this inequality is $\mathcal{O}(0.1\lambda \sim 10\text{nm})$. However this condition may be violated for non-relativistic electrons (E_e lower than 100 keV) and/or angles of incidence $\alpha \rightarrow 90^\circ$.

E. Radiation field from charged particle bunch with azimuthal current

Consider a particle moving at the angle ξ to the z -axis. If its position in the plane $z = 0$ is given by the vector $\boldsymbol{\rho} = \rho(\sin \varphi, \cos \varphi, 0)$, then its velocity vector is

$$\mathbf{u} = u(-\sin \xi \cos \varphi, \sin \xi \sin \varphi, \cos \xi).$$

Note that φ refers to characterize the position of the particle, while ϕ is still used to denote the azimuthal angle of the emitted photon. The current thus acquires the azimuthal component, see Fig. 2. For oblique incidence on a screen, the expressions turn into

$$\boldsymbol{\rho} \rightarrow \rho \mathbf{e}_\rho = \rho \begin{pmatrix} \sin \varphi \cos \alpha \\ \cos \varphi \\ -\sin \varphi \sin \alpha \end{pmatrix}, \quad \mathbf{u} \rightarrow u \begin{pmatrix} \cos \xi \sin \alpha - \sin \xi \cos \varphi \cos \alpha \\ \sin \xi \sin \varphi \\ \cos \xi \cos \alpha + \sin \xi \cos \varphi \sin \alpha \end{pmatrix}. \quad (39)$$

Here α is the angle between the symmetry axis of the helical motion (we have in mind subsequent integration over φ) and the normal to the boundary.

Since we assume that the charged particles following these trajectories have no intrinsic magnetic moment, the TR is calculated in the standard way. We only note that the Fourier-transform of the current density for a trajectory with a given $\boldsymbol{\rho}$ acquires a phase factor

$$\mathbf{j}_e(\mathbf{q}, \omega) = \frac{e}{(2\pi)^3} \mathbf{u} \delta(\omega - \mathbf{q} \cdot \mathbf{u}) e^{-i\mathbf{q} \cdot \boldsymbol{\rho}}, \quad (40)$$

We then find the radiation field for each $\boldsymbol{\rho}$ and integrate it over all polar angles φ as well as with respect to ρ within certain limits. This effectively corresponds to summing over large number of particles distributed homogeneously over a certain annular region. One can then recycle the formulas from the previous subsection by setting $\mu = 0$ there, and represent the out-of-plane and in-plane components for the radiation field as

$$H_{out}^R = \int_0^{2\pi} \frac{d\varphi}{\pi} \int_{R_{min}}^{R_{max}} \frac{\rho d\rho}{R_{max}^2 - R_{min}^2} \mathcal{N} \left[-\sin\theta \frac{\omega}{u_z} (\mathbf{k} \cdot \mathbf{u} - \omega(1 - \beta_z^2)) \pm \sqrt{\varepsilon_\theta} \left(\frac{\omega}{c}\right)^2 (u_y \sin\phi + u_x \cos\phi) \right], \quad (41)$$

$$H_{in}^R = \int_0^{2\pi} \frac{d\varphi}{\pi} \int_{R_{min}}^{R_{max}} \frac{\rho d\rho}{R_{max}^2 - R_{min}^2} \mathcal{N} \sqrt{\varepsilon} \left(\frac{\omega}{c}\right)^2 (u_x \sin\phi - u_y \cos\phi), \quad (42)$$

where

$$\mathcal{N} = \pm \frac{e\omega}{2\pi c^2} (\varepsilon - 1) \frac{e^{i\sqrt{\varepsilon}r\omega/c}}{r} \frac{e^{-i\rho(\mathbf{k}_\perp \cdot \mathbf{e}_\rho + e_{\rho,z}(\omega - \mathbf{k}_\perp \cdot \mathbf{u})/u_z)}}{(\omega - \mathbf{k} \cdot \mathbf{u})(\mathbf{k}_\perp^2 + (\omega - \mathbf{k}_\perp \cdot \mathbf{u})^2/u_z^2 - \omega^2/c^2)} \quad (43)$$

Integration over ρ is trivial here, while integration over φ will be performed numerically. The radiated energy is also found as in the previous case.

IV. NUMERICAL RESULTS

A. Benchmark case

We start presenting numerical results with the following choice of parameters, which we call the benchmark case. The medium is chosen to be aluminium (the permittivity data are taken from [36]), the incidence angle is $\alpha = 70^\circ$, the electron energy is $E_e = 300$ keV. The TR lobes are broad functions of θ_1 and θ_2 , and are shown in Fig. 3 at $\ell = 0$.

If we are aiming at detection of asymmetry in θ_2 , we should focus on such a θ_1 region in which the θ_2 -dependence has a two-bump structure. For this purpose, we consider below θ_2 -distributions integrated over a θ_1 -region centered at some value $\bar{\theta}_1$; specifically, we choose the integration region $[\bar{\theta}_1 - 10^\circ, \bar{\theta}_1 + 10^\circ]$ spread. Then, at non-zero and large ℓ , we expect these two bumps to differ from each other. In Fig. 4 we show the spectral-angular distribution of the emitted energy for the forward and backward TR as a function of θ_2 for fixed $\bar{\theta}_1 = -40^\circ$ and $\hbar\omega = 5$ eV. These choices constitute our benchmark case.

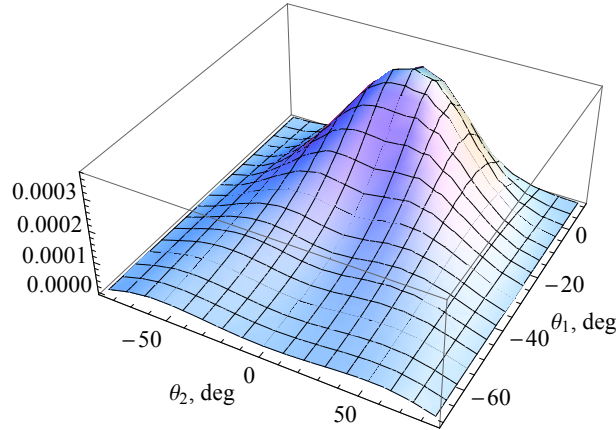


FIG. 3: (Color online.) Distribution of the emitted TR energy over angles θ_1 and θ_2 in the benchmark case ($\alpha = 70^\circ, \gamma = 1.59, \hbar\omega = 5$ eV) at $\ell = 0$.

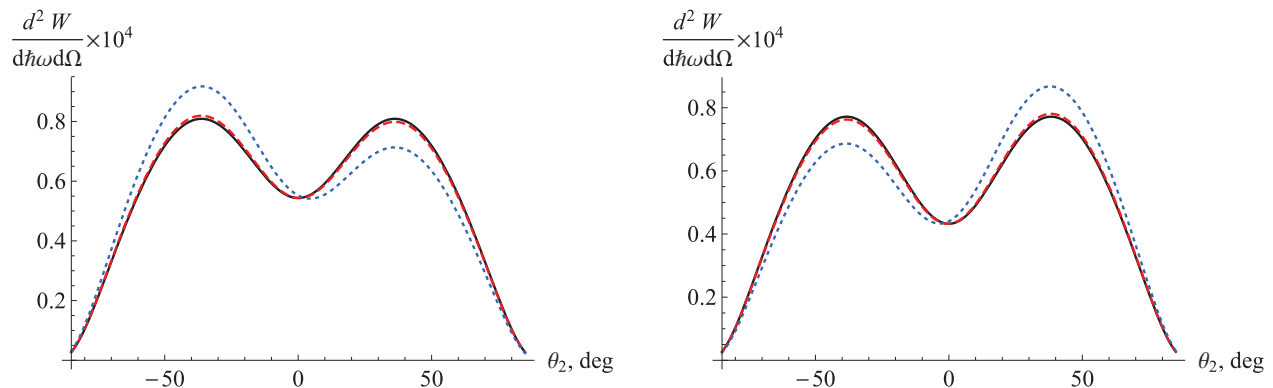


FIG. 4: (Color online.) Distribution in θ_2 of the forward (left plot) and backward (right plot) TR for the benchmark case ($\alpha = 70^\circ, \bar{\theta}_1 = -40^\circ, \gamma = 1.59, \hbar\omega = 5$ eV) at $\ell = 0$ (solid black curve), 1000 (dashed red curve) and 10000 (blue dotted curve).

Note that the θ_2 -distribution becomes strongly distorted at $\ell \sim 10^4$, which is consistent with the parameter $x_\ell \sim 10^{-5} \cdot \ell$ governing the magnitude of the left-right asymmetry. For $\ell < 10^3$, the asymmetry is not easily discernible by eye and should be extracted via (11). Its value is shown in Fig. 5. As expected, it shows a nearly perfect proportionality to ℓ .

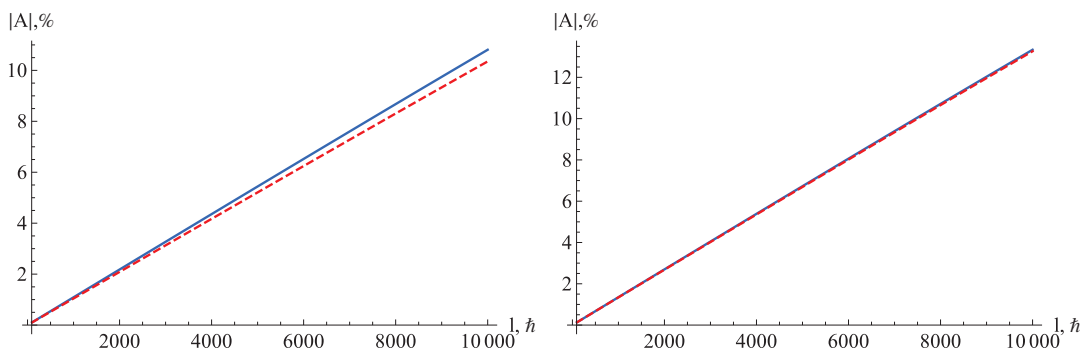


FIG. 5: (Color online.) The magnitude of asymmetry A in the benchmark case ($\bar{\theta}_1 = -40^\circ$) as a function of ℓ for $\hbar\omega = 5$ eV (left) and $\hbar\omega = 10$ eV (right). The blue solid line and the red dashed one correspond to forward TR and backward TR, respectively.

Finally, using the absolute value of the emitted energy distribution shown in Fig. 3 and Fig. 4, one can estimate that the average number of emitted UV photons (say, in the range 3 – 10 eV) per one incident electron is $n_\gamma/n_e \sim \mathcal{O}(10^{-5} - 10^{-4})$. For a current of 1 nA it converts to $\mathcal{O}(10^5 - 10^6)$ of TR photons per second.

B. Dependences

Next, we show in Fig. 6 how the θ_2 -distribution changes upon variation of incidence (α) and detection (θ_1) angles. One sees that the two-bump structure becomes more pronounced for grazing incidence (α close to 90°) and larger negative θ_1 . This is convenient for detection of (backward) TR, as the photons are to be detected at large angles $\sim 100^\circ$ from the electron beam.

The spectral dependence of the asymmetry is shown in Figs. 7, 8. Note that the initial rise $|A| \propto \hbar\omega$ is quickly tamed in near UV due to frequency dispersion of the permittivity, which makes this region best for detection of the effect. Note that we employ the simplest definition of the asymmetry (11), whereas the alternative definition, (10) with $f(\theta_2) = \sin(\theta_2)$, yields even larger values of A (rise up to $\sim 20\%$ for benchmark case).

To quantify the visibility of the asymmetry, we introduce its statistical significance S . It shows how the “true” extracted asymmetry compares to a typical “fake” asymmetry which might arise in a perfectly symmetric distribution

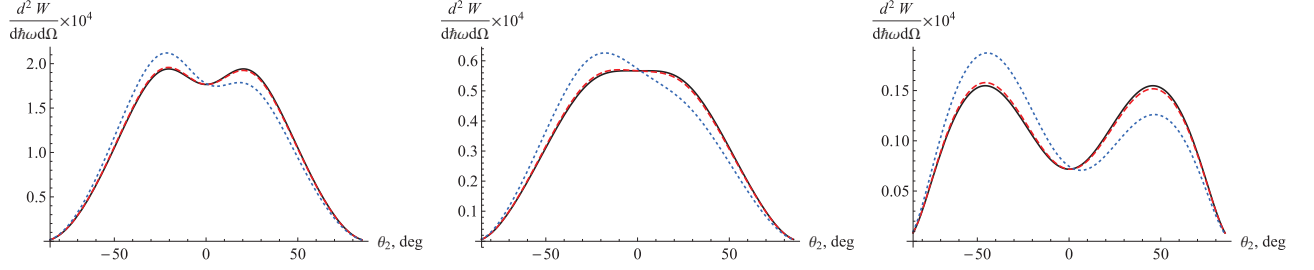


FIG. 6: (Color online.) Forward TR θ_2 -distributions for three other choices of angles: $\alpha = 70^\circ$, $\bar{\theta}_1 = -20^\circ$ (left), $\alpha = 80^\circ$, $\bar{\theta}_1 = -40^\circ$ (middle), $\alpha = 80^\circ$, $\bar{\theta}_1 = -60^\circ$ (right). In all cases $\ell = 0$ is the solid black curve, $\ell = 1000$ is the dashed red curve, and $\ell = 10000$ is the blue dotted curve.

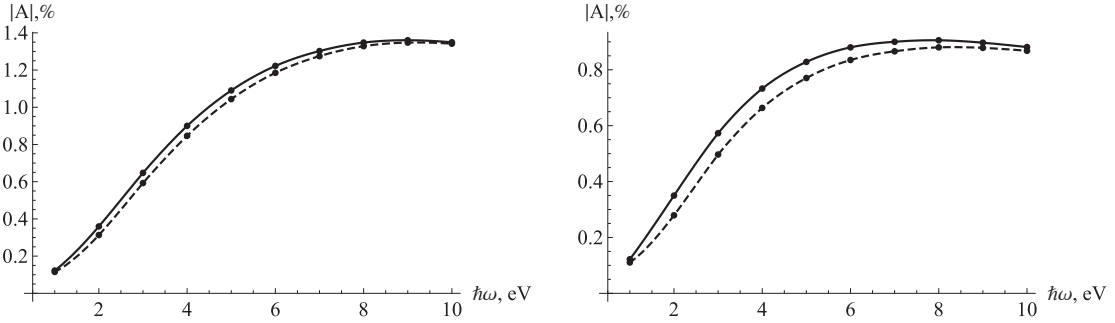


FIG. 7: The magnitude of left-right asymmetry for forward (solid line) and backward (dashed line) TR as a function of the photon energy at the incidence angle $\alpha = 70^\circ$ and $\ell = 1000$. The two plots correspond to $\bar{\theta}_1 = -40^\circ$ (left plot) and $\bar{\theta}_1 = -20^\circ$ (right plot).

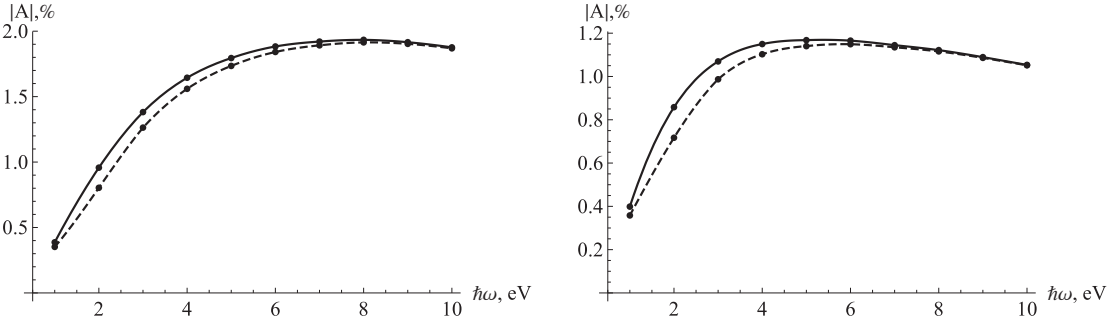


FIG. 8: The magnitude of left-right asymmetry for forward (solid line) and backward (dashed line) TR as a function of the photon energy at the incidence angle $\alpha = 80^\circ$ and $\ell = 1000$. The two plots correspond to $\bar{\theta}_1 = -60^\circ$ (left plot) and $\bar{\theta}_1 = -40^\circ$ (right plot).

due to a statistical fluctuation. If the asymmetry is calculated according to (10) with the weight function $f(\theta_2)$, and if the total number of electrons incident integrated over certain time is N_e , then we define the weighted total photon count N_γ as

$$N_\gamma(\bar{\omega}) = N_e \int \frac{d\omega}{\omega} \int d\Omega |f(\theta_2)| \frac{d^2 W}{d\omega d\Omega}. \quad (44)$$

The spectral integral here extends over a certain region centered as $\bar{\omega}$ (for the estimates below, we use 1 eV-wide

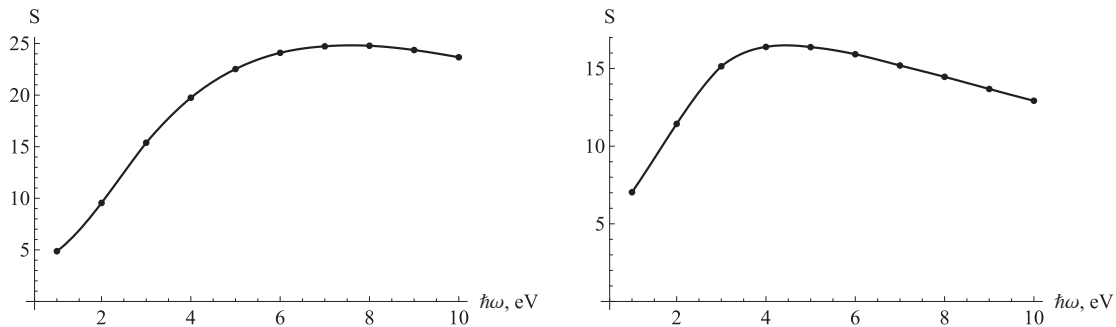


FIG. 9: Statistical significance of the backward TR left-right asymmetry for $\ell = 1000$, based on statistics of $5 \cdot 10^{12}$ electrons and assuming 10% quantum efficiency for the photon detector. Left panel: $\alpha = 70^\circ, \theta_1 = -40^\circ$, right panel: $\alpha = 80^\circ, \theta_1 = -60^\circ$. Integration in θ_2 goes over $\pm(10^\circ, 90^\circ)$.

bins). The left-right asymmetry of the counts is then

$$\Delta N_\gamma(\bar{\omega}) = N_e \int \frac{d\omega}{\omega} \int d\Omega f(\theta_2) \frac{d^2 W}{d\omega d\Omega}. \quad (45)$$

The expected mean value of statistical fluctuation of ΔN_γ is $\sqrt{N_\gamma}$. Therefore, the statistical significance is defined by

$$S(\bar{\omega}) = \frac{\Delta N_\gamma(\bar{\omega})}{\sqrt{N_\gamma(\bar{\omega})}}. \quad (46)$$

The true statistical significance of the count difference detected in an experiment will certainly be smaller due to systematic uncertainties. However $S(\bar{\omega})$ still gives a good idea of the needed integration time and of the $\bar{\omega}$ region optimal for the asymmetry detection. We plot this quantity in Fig. 9 for the statistics of $5 \cdot 10^{12}$ incident electrons, which corresponds to the integration time of ≈ 15 min at the current of 1 nA. The quantum efficiency of the photon detector is assumed to be 10%. We see that at these parameters the asymmetry should be very visible, and the optimal frequency range is near-UV. The values shown in Fig. 9 correspond to $f(\theta_2) = \text{sgn}(\theta_2)$. The analogous choice, $f(\theta_2) = \sin(\theta_2)$, yields the values of S lower by $\sim 20\%$.

As for the sensitivity of the results on the values of permittivity, we only mention here that this dependence is rather weak provided the substance under consideration has a prominent absorption, ϵ'' . We obtain asymmetries of the same order of magnitude by varying ϵ' and ϵ'' over at least one order of magnitude. Therefore, we expect the similar visibility from other metals.

V. DISCUSSION

A. Experimental feasibility

In this section we provide some rough estimates which show that the effect can in principle be observed with today technology and requires only moderate adjustments in the electronic microscopes currently used for vortex electron generation.

The key issue enabling the observations we suggest is creation of vortex electrons with large OAM. The figure of merit here is not the largest OAM by itself, but the OAM value at the first diffraction peak (higher order peaks are strongly suppressed in intensity). The maximal value achieved so far is 25 [17]; a tenfold increase in this value is highly desirable. This will certainly pose challenge in manufacturing the appropriate diffraction gratings, but these values seem to be within technological limits. Indeed, a typical aperture available at the position of condenser lens is of order of hundred microns, while the smallest features which can be accurately etched in the grating are of tens of nanometers.

It might also be possible to create very high OAM vortex electrons using the recently demonstrated technique of electron scattering on the effective magnetic monopole, [37]. In this experiment, the ring-shape non-vortex electron wave passes through an open end of a magnetic whisker or a nanoscaled solenoid, whose field is well approximated

locally by a magnetic monopole field, and it acquires vorticity. The value of OAM is determined by the effective magnetic charge of the monopole, which can in principle be made very large.

It must be stressed that our suggestion does not require the vortex electrons to be in a state of a definite value of ℓ . Quite to the contrary, the OAM can be spread over a certain rather broad range, and the effect will still be there. Even if the transverse profile of the electron state becomes distorted, it does not have any sizable effect on asymmetry because all transverse shifts remain much smaller than λ . This makes our predictions robust against imperfections of the experimental method of generating high-OAM vortex electrons.

A similar conclusion holds for another distortion effect. It can be expected that higher order phase vortices are inherently unstable. Upon propagation in a magnetic lense system with stray fields, they might split into a compact “cloud” of vortices of topological order one. This possibility however does not affect the predicted asymmetry if the “cloud” stays compact, $\ll \lambda$.

The second delicate issue is the alignment of the photon detectors. We propose to place two identical large aperture detectors symmetrically on the two sides of the electron incidence plane. They do not even have to be pixelated, because the quantity to be measured is the asymmetry between the left and right detectors. All instrumentation alignment should be performed with a relative accuracy better than the estimated asymmetry.

If achieving an accurate symmetric alignment proves difficult, one can then fix the instrumentation and simply change the sign of the OAM of vortex electrons. This can be done by tilting the grating without any mechanical manipulation to the target or to detectors. One should then observe the sign change in the asymmetry.

The third issue concerns the expected energy of TR. Using our estimates of $n_\gamma \sim \mathcal{O}(10^{-4})$ photons per electron and taking a current of 1 nA, which is easily achievable in microscopes producing vortex electrons, one can expect about 10^5 photons per second detected by photocathods with quantum efficiency 10%. A sufficiently long integration time will lead to 10^8 photons, and with this statistics a left-right asymmetry of the order $A \sim 0.1\%$ can be reliably detected.

Finally, let us comment on coherence issues. The coherence condition for radiation (focusing the electron beam to spots much smaller than the wavelength of the emitted light) can be easily achieved with existing devices. Focusing a vortex beam with small ℓ to angstrom scale spots has been demonstrated [29], and one can expect that electrons with $\ell = 1000$ to submicron scales should also be feasible.

Longitudinal extent of the individual electron wave function should also be below optical wavelength, which means that the longitudinal coherence of the electron beam should not be too good. This can be cast in the form of requirement that the monochromaticity of the electrons should be *worse* than a few eV.

B. The effect in other forms of polarization radiation

In this paper we have discussed possibilities for detecting the interference term $dW_{e\mu}$ in the Cherenkov radiation and transition radiation. These phenomena represent, in fact, two particular cases of the general process of polarization radiation. Rather simple considerations allow one to estimate the magnitude of the similar effect in other processes like, for instance, diffraction radiation and Smith-Purcell radiation. Indeed, for an observer located far enough from the target (in the wave zone), the radiation arises as a result of a distant collision of a (vortex) electron with a point-like dipole moment $d(\omega)$. Irrespectively of the target shape, the radiation field in the wave zone is (integration is over the target volume)

$$\mathbf{H}^{PR} \propto \mathbf{e}_k \times \int_V d^3r \mathbf{d}(\mathbf{r}, \omega) e^{-i(\mathbf{k}\mathbf{r})} \propto \mathbf{e}_k \times \mathbf{d}(\omega) \quad (47)$$

since in the dipole approximation $\mathbf{j}^{pol} = -i\omega\mathbf{d}$. Roughly speaking, it is the explicit expression for the dipole moment \mathbf{d} that only makes difference in different types of polarization radiation. As a result, the product

$$\mathbf{e}_k \cdot [\boldsymbol{\mu}\mathbf{d}]$$

or $\mathbf{e}_k \cdot [\mathbf{e}_u\mathbf{d}]$ (since $\boldsymbol{\mu} \parallel \mathbf{u}$) will govern the effect (with \mathbf{d} instead of the normal \mathbf{n}). From this, it is immediately clear that the interference effect is absent for Cherenkov radiation (even for arbitrary complex $\varepsilon(\omega)$), for transition radiation at normal incidence, and also for diffraction radiation when a particle moves *nearby* a metallic foil, perpendicular to the surface, but does not intersect it (for a detailed description see e.g. [2]). The effective dipole moment in most cases of practical interest is perpendicular to the target surface [4], so in all the geometries mentioned $\mathbf{d} \parallel \mathbf{u}$. On the contrary, the effect will exist when a particle moves *obliquely* with respect to the target surface in diffraction radiation problem or even when it moves nearby a metallic grating like in the Smith-Purcell radiation. In all these geometries one could expect the same angular asymmetry, which should increase as the angle between \mathbf{d} and \mathbf{u} grows, and its

numerical value will be of the same order as in TR case. Finally, one can note that when dealing with other types of polarization radiation the actual dielectric properties of the target materials and the frequency dispersion are highly important, and they can be taken into account with the approach developed in [4].

One could also mention that if vortex electrons with the high values of OAM were created, detection of the radiation asymmetry could serve as a diagnostic tool allowing one to obtain the ℓ value of the beam. Such a diagnostics could be done non-invasively when using diffraction radiation from a rectangular plate instead of transition radiation. The former has the same angular distributions in the θ_2 -plane as in the TR case considered here, but the beam characteristics stay undisturbed during the emission process (see e.g. [2]).

VI. CONCLUSIONS

Recently created vortex electrons carrying large orbital angular momentum ℓ and, therefore, a large OAM-induced magnetic moment are an ideal tool to investigate influence of magnetic moment on various forms of polarization radiation. This influence has been discussed theoretically since long ago but up to now has never been studied experimentally. As the magnetic moment contribution is parametrically suppressed by small parameter $x_\ell = \ell\hbar\omega/E_e$, one can hope to detect it only via its interference with the charge contribution (which can be extracted via angular asymmetry), but even here one must strive for largest achievable ℓ .

In this paper, we investigated this effect for various forms of polarization radiation. We showed absence of the interference term for Cherenkov radiation, studied in detail the interference and the asymmetry for transition radiation, and commented possibility to observe this effect for other forms of PR. In particular, we argued that for $\ell = 100-1000$, the asymmetry in TR can be of order 0.1%–1%, which could be measurable with existing technology. Simultaneously, it offers a novel method of measuring large OAM in electron vortex beams.

Acknowledgments

I.P.I. acknowledges grants RFBR 11-02-00242-a and RF President grant for scientific schools NSC-3802.2012.2. D.V.K. acknowledges grants of the Russian Ministry for Education and Science within the program “Nauka” and Nos. 14.B37.21.0911, 14.B37.21.1298. The authors are grateful to J. Verbeeck and members of his team at the Antwerpen University for discussions on experimental feasibility of the proposed measurement.

-
- [1] M. I. Ryazanov, *Electrodynamics of continuous medium* (Nauka, Moscow 1984), in Russian.
 - [2] A. P. Potylitsyn, M. I. Ryazanov, M. N. Strikhanov, A. A. Tishchenko, *Diffraction radiation from relativistic particles*, STMP 239 (Springer, Berlin Heidelberg 2010).
 - [3] M. Ya. Amusia, *Radiat. Phys. Chem.* **75**, 1232 (2006).
 - [4] D. V. Karlovets, *J. Exp. Theor. Phys.* **113**, 27 (2011).
 - [5] V. A. Bordovitsyn, I. M. Ternov, and V. G. Bagrov, *Phys. Usp.* **38**, 1037 (1995).
 - [6] A. Lobanov, A. Studenikin, *Phys. Lett. B* **564**, 27 (2003); A. Grigoriev, S. Shinkevich, A. Studenikin, et al., *Grav. & Cosm.* **14**, 248 (2008).
 - [7] M. Sakuda, *Phys. Rev. Lett.* **72**, 804 (1994); M. Sakuda, Y. Kurihara, *Phys. Rev. Lett.* **74**, 1284 (1995);
 - [8] A. Gover, *Phys. Rev. Lett.* **96**, 124801 (2006); *Phys. Rev. ST - Accel. Beams* **9**, 060703 (2006).
 - [9] I. M. Frank, *Sov. Phys. Usp.* **27**, 772 (1984).
 - [10] V. L. Ginzburg and V. N. Tsytovich, *Transition Radiation and Transition Scattering* (Nauka, Moscow, 1984; Adam Hilger, New York, 1990); *Phys. Rept.* **49**, 1 (1979).
 - [11] S. A. Belomestnykh, A. E. Bondar, M. N. Egorychev *et al.*, *Nucl. Instrum. Meth. A* **227**, 173 (1984).
 - [12] D. Dutta, *J. Phys. Conf. Ser.* **295**, 012141 (2011).
 - [13] K. Kirsebom, U. Mikkelsen, E. Uggerhøj *et al.*, *Phys. Rev. Lett.* **87**, 054801 (2001).
 - [14] K. Yu. Bliokh, Yu. P. Bliokh, S. Savel'ev, F. Nori, *Phys. Rev. Lett.* **99**, 190404 (2007).
 - [15] M. Uchida and A. Tonomura, *Nature* **464**, 737 (2010);
 - [16] J. Verbeeck, H. Tian, P. Schlattschneider, *Nature* **467**, 301 (2010);
 - [17] B. J. McMorran et al, *Science* **331**, 192 (2011).
 - [18] K. Saitoh, Y. Hasegawa, N. Tanaka, and M. Uchida, *J. Electron. Microsc. (Tokyo)* **61**, 171 (2012).
 - [19] K. Yu. Bliokh, M. R. Dennis, F. Nori, *Phys. Rev. Lett.* **107**, 174802 (2011).
 - [20] I. P. Ivanov, D. V. Karlovets, arXiv:1304.0359 [physics.optics].
 - [21] M. Ya. Amus'ya, A. S. Baltentov, A. A. Paiziev, *JETP Lett.* **24**, 332 (1976).

- [22] V. V. Syshchenko, N. F. Shul'ga, J. Surf. Investig. **1**, 217 (2007); N. F. Shul'ga, V. V. Syshchenko, J. Phys.: Conf. Ser. **236**, 012010 (2010).
- [23] A. A. Tishchenko, A. P. Potylitsyn, M. N. Strikhanov, Phys. Rev. E **70**, 066501 (2004); Phys. Lett. A **359**, 509 (2006).
- [24] V. L. Ginzburg and I. M. Frank, J. Phys. (USSR) **9**, 353 (1945) [Zh. Eksp. Teor. Fiz. **16**, 15 (1946)].
- [25] V. E. Pafomov, Proc. P.N. Lebedev Phys. Inst. **44**, 25 (1971).
- [26] L. D. Landau, E. M. Lifshitz, L. P. Pitaevskii, *Electrodynamics of continuous media* (Butterworth-Heinemann, Oxford, 1995), 2nd ed.
- [27] A. S. Konkov, A. P. Potylitsyn, and V. A. Serdyutskii, Russian Physics Journal **54**, 1249 (2012).
- [28] A. S. Konkov, A. P. Potylitsyn and M. S. Polonskaya, arXiv:1304.7363 [physics.acc-ph].
- [29] J. Verbeeck et al, Appl. Phys. Lett. **99**, 203109 (2011).
- [30] U. D. Jentschura and V. G. Serbo, Phys. Rev. Lett. **106**, 013001 (2011); U. D. Jentschura and V. G. Serbo, Eur. Phys. J. **C71**, 1571 (2011).
- [31] D. V. Karlovets, Phys. Rev. A **86**, 062102 (2012).
- [32] K. Bliokh, P. Schattschneider, J. Verbeeck, F. Nori, Phys. Rev. **X 2**, 041011 (2012); G. Guzzinati, P. Schattschneider, K. Bliokh, F. Nori, J. Verbeeck, Phys. Rev. Lett. **110**, 093601 (2013).
- [33] M. I. Ryazanov, Sov. Phys.-JETP **5**, 1013 (1957); **7**, 869 (1958).
- [34] V. G. Baryshevsky, I. D. Feranchuk, A. P. Ulyanenko, *Parametric X-ray radiation in crystals. Theory, experiments, applications*. (Springer-Verlag, Berlin-Heidelberg, 2006).
- [35] M. I. Ryazanov, JETP Lett. **39**, 698 (1984).
- [36] A. D. Rakić, Appl. Optics **34**, 4755 (1995).
- [37] A. Béché, R. Van Boxem, G. Van Tendeloo, J. Verbeeck, arXiv:1305.0570 [physics.ins-det].
- [38] We use integration measures $d^3x/(2\pi)^3$ and d^3q .